Applied Catalysis A: General 480 (2014) 100–107

Contents lists available at ScienceDirect

Applied Catalysis A: General

journal homepage: www.elsevier.com/locate/apcata

# Preparation and characterization of core–shell polyaniline/mesoporous $Cu_2O$ nanocomposites for the photocatalytic oxidation of thiophene

R.M. Mohamed [a,b,c,*], E.S. Aazam [a]

[a] Chemistry Department, Faculty of Science, King Abdulaziz University, P.O. Box 80203, Jeddah 21589, Saudi Arabia
[b] Nanostructured Material Division Advanced Materials Department, Central Metallurgical R&D Institute, Helwan, 11421 Cairo, Egypt
[c] Center of Excellence in Environmental Studies, King Abdulaziz University, P.O. Box 80216, Jeddah 21589, Saudi Arabia

ARTICLE INFO

*Article history:*
Received 14 December 2013
Received in revised form 20 April 2014
Accepted 22 April 2014
Available online 1 May 2014

*Keywords:*
Polyaniline
Mesoporous $Cu_2O$
Visible photocatalyst
Thiophene removal

ABSTRACT

Polyaniline/mesoporous $Cu_2O$ core–shell nanocomposites with different mass ratios of polyaniline/mesoporous $Cu_2O$ were prepared using a hydrothermal method. For comparison, $Cu_2O$ nanoparticles and polyaniline/$Cu_2O$ nanoparticles were also prepared using a hydrothermal method. The catalytic performance of the samples during the photocatalytic oxidation of thiophene under visible-light irradiation was determined. The surface areas of the mesoporous and nanoparticulate $Cu_2O$ materials were 140 and 40 $m^2$/g, respectively. Adding polyaniline to mesoporous and nanoparticulate $Cu_2O$ decreases the surface areas of the nanoparticles to 120 and 32 $m^2$/g, respectively. TEM images reveal that the mesoporous and nanoparticulate $Cu_2O$ materials occur as uniform microspheres and spherical nanoparticles, respectively. The polyaniline/mesoporous $Cu_2O$ and polyaniline/$Cu_2O$ nanoparticles are core–shell and spherical nanoparticles, respectively. The photocatalytic degradation of thiophene under visible-light irradiation while using 4% polyaniline/mesoporous $Cu_2O$ was 2.87, 2.20, and 1.34 times more effective than that observed when using $Cu_2O$ nanoparticles, polyaniline/$Cu_2O$ nanoparticles, and mesoporous $Cu_2O$, respectively.



## 1. Introduction

$Cu_2O$ has attracted significant attention due to its potential applications in photocatalysis [1–4], CO oxidation [5], sensing [6], antibacterial agents [7–10], and solar energy conversion [11]. The photocatalytic properties of $Cu_2O$ depend on its morphology and microstructure. Many researchers have improved the photocatalytic properties of $Cu_2O$ by varying its morphology [12–20].

Recently, many researchers have used conductive polymers (polyaniline, polythiophene, and polypyrrole) as sensitizers to expand the absorption of photocatalysts in the visible region. The photocatalytic activity of a semiconductor/conductive polymer composite under visible light is high due to the visible-light absorption of the conductive polymer, whereas the charge separation of electron–hole (e–h) pairs leads to heterojunctions between the conductive polymer and the semiconductor. In a previous study, PANI/$TiO_2$ was prepared using a chemisorption method [21]. The authors observed that the photocatalytic activity of the PANI/$TiO_2$ composite under visible light surpasses that of $TiO_2$ in terms of the degradation of phenol or dyes. The low visible-light-harvesting efficiency exhibited by the conductive polymer limits its photocatalytic activity. Many methods have been used to extend the absorption of sanitized semiconductor hybrids in the visible region, including using a semiconductor with a small particle size and a high surface area. This method is effective because the high surface area increases the uptake for the sensitizer and enhances the visible absorption. Additionally, small particle sizes enhance e–h separation [22–27]. Increasing the optical path length of photons in photocatalysts is another method used to increase visible-light-harvesting efficiency. This method has been realized through the synthesis of microspheres and photonic crystals [26–31]. Therefore, preparing a mesoporous semiconductor/conductor polymer composite should increase the visible-light-harvesting efficiency by increasing the surface area and optical path length of photons. In this work, we prepared a polyaniline/mesoporous $Cu_2O$ core–shell nanocomposite and a polyaniline/$Cu_2O$ nanoparticle composite for comparison to evaluate the materials' photocatalytic degradation of thiophene under visible-light irradiation.

* Corresponding author at: Chemistry Department, Faculty of Science, King Abdulaziz University, P.O. Box 80203, Jeddah 21589, Saudi Arabia. Tel.: +966 540715648; fax: +966 2 6952292.
*E-mail address:* mhmdouf@gmail.com (R.M. Mohamed).

http://dx.doi.org/10.1016/j.apcata.2014.04.039
0926-860X/

## 2. Experimental

### 2.1. Synthesis of photocatalyst

#### 2.1.1. Synthesis of mesoporous $Cu_2O$ (M-$Cu_2O$)

Mesoporous copper (I) oxide was prepared as follows: the appropriate amount of $CuCl_2{\cdot}2H_2O$ was dissolved in deionized water that was kept cool in an ice-water bath. Aqueous ammonium sulfate and urea were added, and the mixture was stirred for 2 h. Subsequently, an equal volume of ethanol was added dropwise to the solution. The molar ratio of the reactants was as follows: $1CuCl_2{:}80H_2O{:}20EtOH{:}1(NH_4)_2SO_4{:}20CO(NH_2)_2$. The resulting solution was maintained at 80 °C for 24 h in an autoclave. Afterward, the sample was filtered, washed several times with ethanol and deionized water, and dried at 60 °C for 24 h. The sample was calcined at 450 °C for 2 h. The obtained sample was named M-$Cu_2O$.

#### 2.1.2. Synthesis of polyaniline/M-$Cu_2O$

We prepared a 0.2 g/L polyaniline solution by dissolving polyaniline in tetrahydrofuran. We added different amounts of M-$Cu_2O$ to 100 mL of this solution. The resulting mixture was sonicated for 30 min and stirred for 24 h. After filtering and washing the suspension several times with water and ethanol, the precipitate was dried at 60 °C for 24 h. By modulating the amount of M-$Cu_2O$ in the 100-mL polyaniline solution, we prepared polyaniline/M-$Cu_2O$ composites with M-$Cu_2O$ mass ratios ranging from 1% to 5%.

#### 2.1.3. Synthesis of nanoparticles $Cu_2O$ (NP-$Cu_2O$)

For comparison, we prepared $Cu_2O$ nanoparticles. The preparation method was as follows: 180 mg of $CuCl_2{\cdot}2H_2O$ and 200 mg of polyethylene glycol (PEG, $M_w$ = 20,000) were dissolved in 200 mL of $H_2O$ and stirred for 30 min. Subsequently, 2 mL of 6 M NaOH was added dropwise to this solution with constant stirring; $Cu(OH)_2$ was produced as a blue precipitate. Next, we added 2 mL of a 14 M hydrazine solution with stirring for 30 min to reduce the $Cu^{2+}$ to $Cu^{1+}$. The resultant red gel was transferred to an autoclave and maintained at 80 °C for 10 h. The sample was filtered and washed several times with distilled water before being dried at 60 °C for 3 h in a vacuum oven. The obtained sample was named NP-$Cu_2O$.

#### 2.1.4. Synthesis of polyaniline/NP-$Cu_2O$

We prepared a 0.2 g/L polyaniline solution by dissolving polyaniline in tetrahydrofuran. We added NP-$Cu_2O$ to 100 mL of this solution. The resulting mixture was sonicated for 30 min and stirred for 24 h. After filtering and washing the suspension several times with water and ethanol, the precipitate was dried at 60 °C for 24 h. PANI/NP-$Cu_2O$ photocatalysts with a 4% mass ratio were synthesized.

### 2.2. Characterization techniques

X-ray diffraction (XRD) analysis was carried out at room temperature with a Bruker D8 Advance diffractometer. The patterns were run with Ni-filtered copper radiation ($\lambda$ = 1.5404 Å) at 30 kV and 10 mA with a scanning speed of 2.5° $min^{-1}$. For phase identification purposes, an automatic JCPDS library search and match procedure was performed.

The specific surface area was calculated by measuring $N_2$ adsorption with a Nova 2000 series Chromatech apparatus at 77 K. Before the measurements, all samples were treated under vacuum at 250 °C for 2 h. The band gap of the samples was identified using UV–vis diffuse reflectance spectra (UV–vis-DRS) measured in air at room temperature from 200 to 800 nm with a UV/vis/NIR spectrophotometer (V-570, JASCO, Japan). The band gap was calculated according to the following formula:

$$E_g\,(\mathrm{eV}) = \frac{1240}{\lambda_g}$$

where the band-gap wavelength ($\lambda_g$, nm) was obtained by extrapolating the wavelength edge of the absorbance peak to the zero line from a diffuse reflectance spectrum. Transmission electron microscopy (TEM) images were recorded with a JEOL-JEM-1230 microscope; the samples were prepared in an ethanolic suspension and ultrasonicated for 30 min. Afterward, a small amount of this solution was applied to a carbon-coated copper grid and dried before loading the sample into the TEM instrument. We performed X-ray photoelectron spectroscopy (XPS) studies using a Thermo Scientific K-ALPHA XPS (England). Photoluminescence (PL) emission spectra were recorded with a fluorescence spectrophotometer (Shimadzu RF-5301). FTIR spectra in transmittance mode were recorded for a solid mixture of sample and KBr in the form of pellets on a JASCO FTIR-6000 spectrometer with a spectral resolution of 2 $cm^{-1}$ and an accumulation of 100 scans at room temperature.

### 2.3. Photocatalytic reaction

A Pyrex reaction cell into which $O_2$ was bubbled was used for the photocatalytic oxidation of thiophene. The thiophene was dissolved in acetonitrile, and the initial sulfur concentration was 600 ppm. Subsequently, a known amount of photocatalyst was dispersed in this solution. A 125-W mercury lamp with a UV cut-off filter was used to irradiate the suspension. Before the suspension was irradiated, it was stirred in the dark for 30 min to establish equilibrium. We maintained the reaction temperature at approximately 11 °C using flowing water. The products and byproducts of the photocatalytic process were analyzed by GC (Agilent 7890). All experiments were repeated at least three times, and average values with error bars are presented.

The ratio of the thiophene removal rate to the incident light intensity was used to calculate the photonic efficiency:

$$\xi = \frac{r \times 100}{I}$$

where $\xi$ is the photonic efficiency (%), $r$ the photo-oxidation rate of thiophene, and $I$ the incident photon flux ($3.37 \times 10^{-6}$ Ein $L^{-1}$ $s^{-1}$).

The quantum yield associated with the thiophene removal rate was determined using the relation $\Phi = \xi/Fs$, where $\xi$ is the

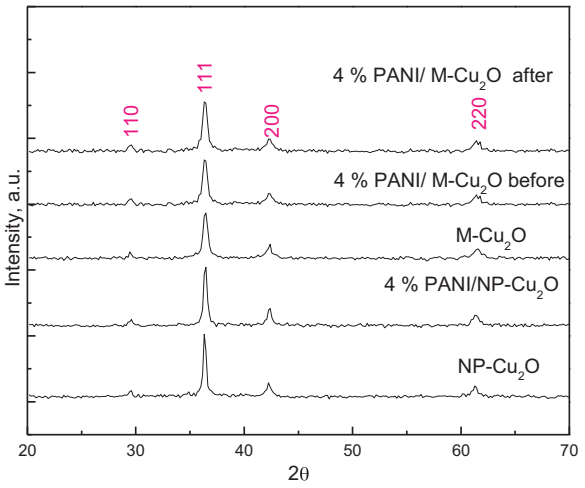


**Fig. 1.** XRD patterns of the NP-$Cu_2O$, 4% PANI/NP-$Cu_2O$, M-$Cu_2O$, and 4% PANI/M-$Cu_2O$ samples before photocatalysis and the XRD pattern of the 4% PANI/M-$Cu_2O$ sample after photocatalysis.

photonic efficiency and *F*s is the fraction of light observed for the tested catalyst.

## 3. Results and discussion

### 3.1. X-ray diffraction analysis

Fig. 1 shows the XRD patterns obtained for the NP-$Cu_2O$, 4% PANI/NP-$Cu_2O$, M-$Cu_2O$, and 4% PANI/M-$Cu_2O$ samples. The results reveal that the cuprite structure of $Cu_2O$ was present in every sample, indicating that there was little change in the $Cu_2O$ lattice structure after modification with PANI. The Scherrer formula was used to determine the crystallite size of the produced samples. The mean crystallite sizes for the NP-$Cu_2O$, 4% PANI/NP-$Cu_2O$, M-$Cu_2O$, and 4% PANI/M-$Cu_2O$ samples were 33, 25, 20, and 16 nm, respectively.

### 3.2. TEM observation

Fig. 2 shows TEM images of the NP-$Cu_2O$, 4% PANI/NP-$Cu_2O$, M-$Cu_2O$, and 4% PANI/M-$Cu_2O$ samples. The NP-$Cu_2O$ and 4% PANI/NP-$Cu_2O$ occur as spherical nanoparticles (Fig. 2a and b). The

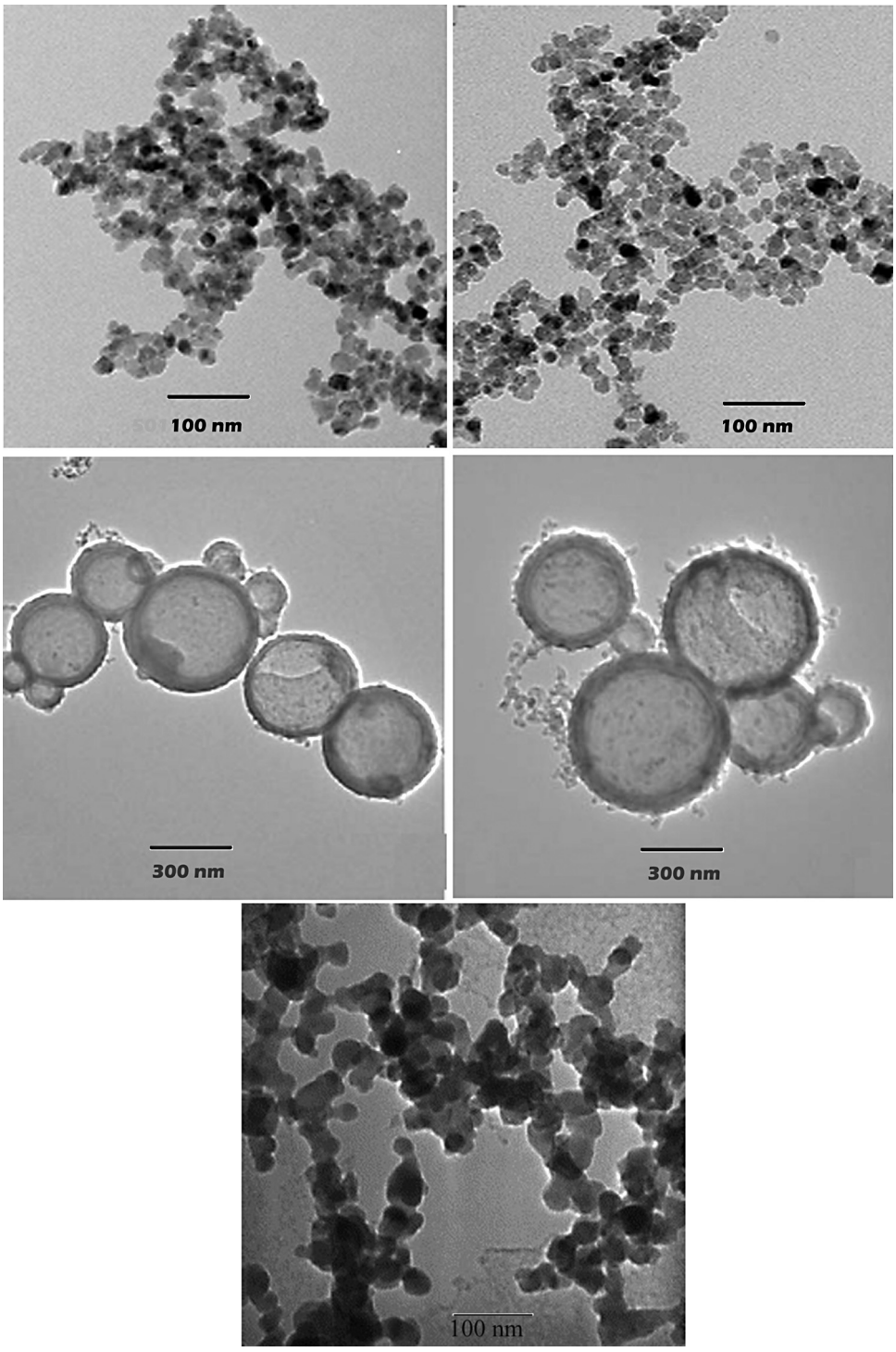


**Fig. 2.** TEM images of the NP-$Cu_2O$ (a), 4% PANI/NP-$Cu_2O$ (b), M-$Cu_2O$ (c), 4% PANI/M-$Cu_2O$ (d), and PANI (f) samples.

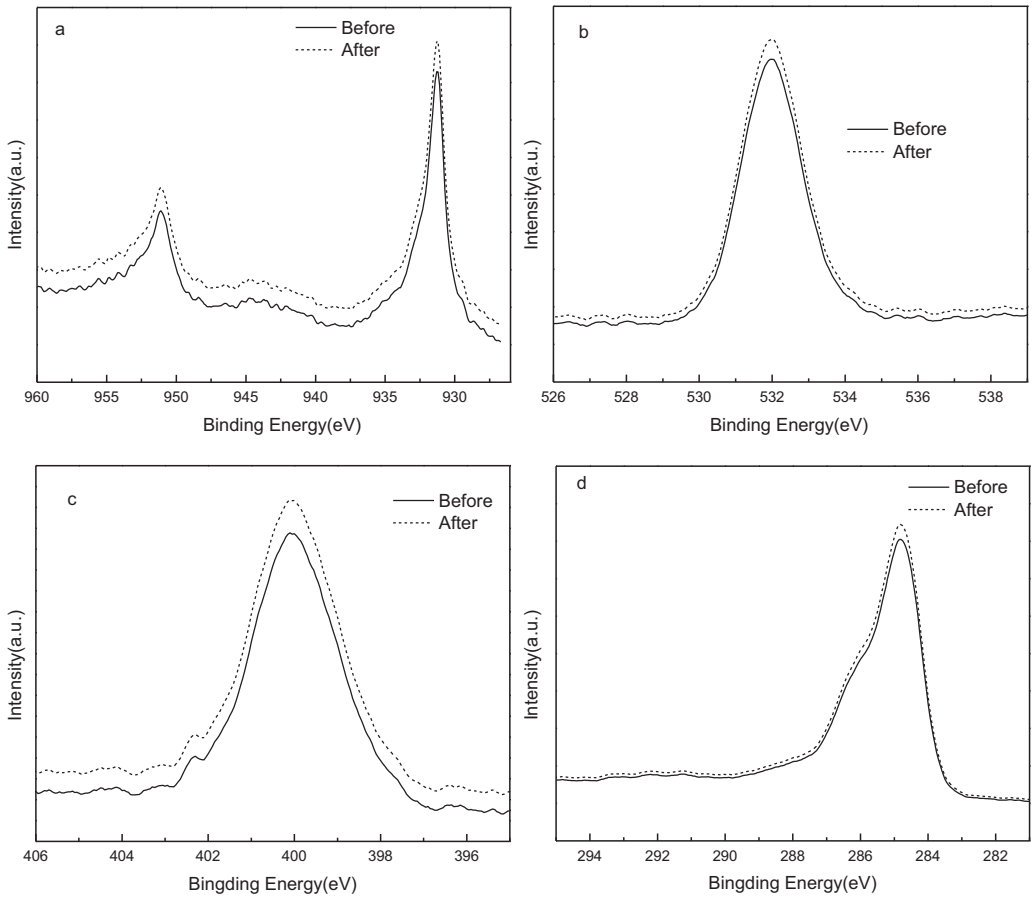


**Fig. 3.** XPS spectra before and after photocatalysis for Cu 2p (a), O 1s (b), N 1s (c), and C 1s.

M-$Cu_2O$ sample is composed of uniform microspheres (Fig. 2c), whereas the 4% PANI/M-$Cu_2O$ particles are nearly the same shape as those constituting the M-$Cu_2O$ sample (Fig. 2d), indicating that PANI exists in a very thin layer on M-$Cu_2O$. Therefore, the microspherical 4% PANI/M-$Cu_2O$ should exhibit high absorption in the visible-light region. Moreover, the results reveal that the particle size of the M-$Cu_2O$ and 4% PANI/M-$Cu_2O$ samples are 200 and 250 nm, respectively. Their core diameters are 400 and 450, respectively, and their shell thicknesses are 30–60 and 35–65 nm, respectively.

### 3.3. XPS analysis

Fig. 3 shows the XPS spectra obtained for the 4% PANI/M-$Cu_2O$ nanocomposite. The peaks at 952.2 and 932.2 eV for Cu 2p1/2 and Cu 2p 3/2 confirm the presence of $Cu^+$ [30] (Fig. 3a). Additionally, the peak at 531.6 eV for O 1s confirms the presence of $O^{2-}$ (Fig. 3b). Therefore, the results confirm the presence of $Cu_2O$. The peaks at 400 and 284.7 eV for N 1s and C 1s, respectively, appear in Fig. 3c and d, respectively, and confirm the presence of aniline in the nanocomposite.

### 3.4. FT-IR analysis

To further confirm the presence of aniline in the nanocomposite, FT-IR analysis was performed, the results of which are shown in Fig. 4 for the PANI and 4% PANI/M-$Cu_2O$ samples. The peaks at 815, 1147, 1245, 1297, 1492, and 1567 $cm^{-1}$ are characteristic for PANI and are visible in the spectrum for the 4% PANI/M-$Cu_2O$ nanocomposite. Therefore, PANI is present in the 4% PANI/M-$Cu_2O$ nanocomposite.

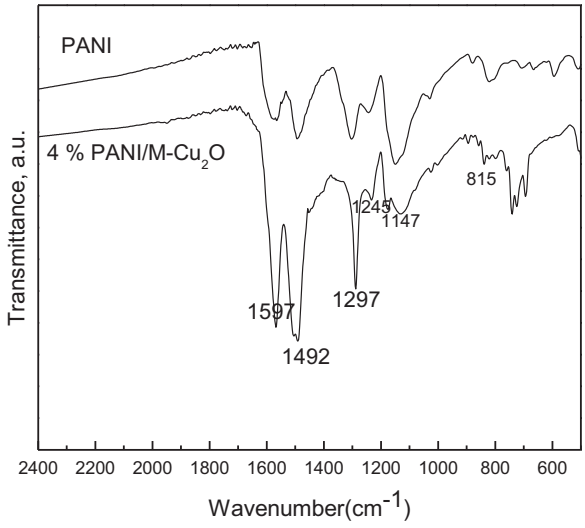


**Fig. 4.** FT-IR spectra of the PANI and 4% PANI/M-$Cu_2O$ samples.

### 3.5. Specific surface area analysis

$N_2$ adsorption–desorption measurements were collected at −196 °C and were used to study the mesoporosity and textural properties of the NP-$Cu_2O$, 4% PANI/NP-$Cu_2O$, M-$Cu_2O$, and 4% PANI/M-$Cu_2O$ samples. Fig. 5 shows the nitrogen

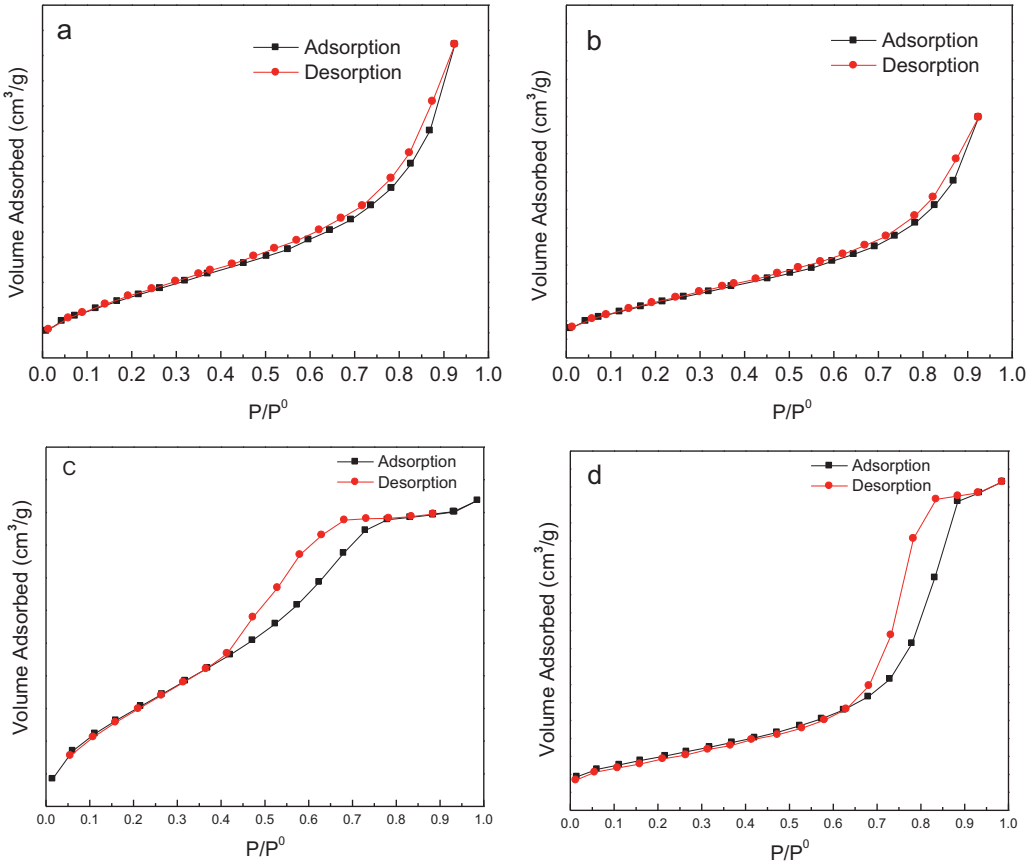


**Fig. 5.** Adsorption–desorption isotherms of the NP-$Cu_2O$ (a), 4% PANI/NP-$Cu_2O$ (b), M-$Cu_2O$ (c), and 4% PANI/M-$Cu_2O$ (d) samples.

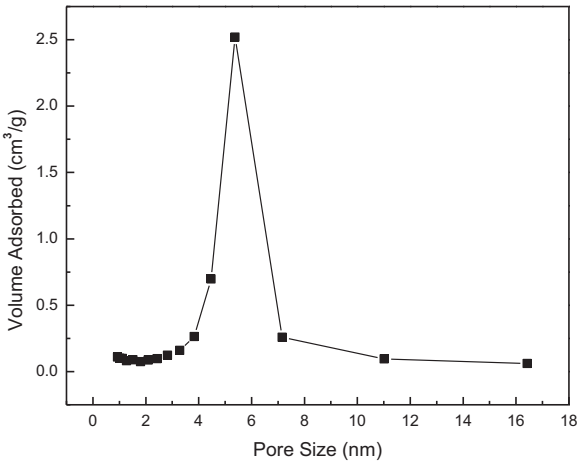


**Fig. 6.** Pore size distribution of 4% PANI/M-$Cu_2O$.

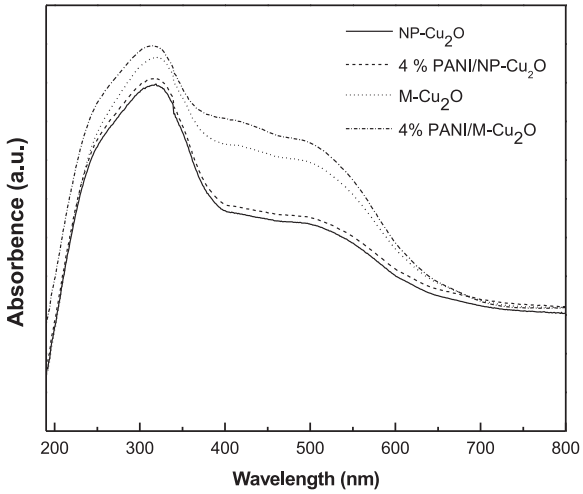


**Fig. 7.** UV–vis spectra of the NP-$Cu_2O$, 4% PANI/NP-$Cu_2O$, M-$Cu_2O$, and 4% PANI/M-$Cu_2O$ samples.

adsorption–desorption isotherms for the NP-$Cu_2O$, 4% PANI/NP-$Cu_2O$, M-$Cu_2O$, and 4% PANI/M-$Cu_2O$ samples. The isotherms for the NP-$Cu_2O$ and 4% PANI/NP-$Cu_2O$ samples are type II isotherms, as shown in Fig. 5a and b. The isotherms for the M-$Cu_2O$ and 4% PANI/M-$Cu_2O$ samples are type IV isotherms, as shown in Fig. 5c and d, confirming the mesoporosity of the M-$Cu_2O$ and 4% PANI/M-$Cu_2O$ nanocomposite samples. The surface areas of $Cu_2O$, 4% PANI/$Cu_2O$, M-$Cu_2O$, and 4% PANI/M-$Cu_2O$ are 40, 32, 140, and 120 $m^2$/g, respectively. The large surface area of 4% PANI/M-$Cu_2O$ should enhance the sample's photocatalytic activity by increasing the number of active sites and enhancing the e–h separation process. Furthermore, Fig. 6 shows the pore size distribution plot calculated using the BJH equation from the desorption–adsorption isotherm of the 4% PANI/M-$Cu_2O$ sample. The results reveal that the 4% PANI/M-$Cu_2O$ sample exhibits a narrow distribution of mesopore sizes, with an average pore diameter of 5 nm.

### 3.6. Optical characterization

Fig. 7 shows the UV–vis spectra obtained for the NP-$Cu_2O$, 4% PANI/NP-$Cu_2O$, M-$Cu_2O$, and 4% PANI/M-$Cu_2O$ samples. The results reveal that the absorption edges of the $Cu_2O$ moved toward longer

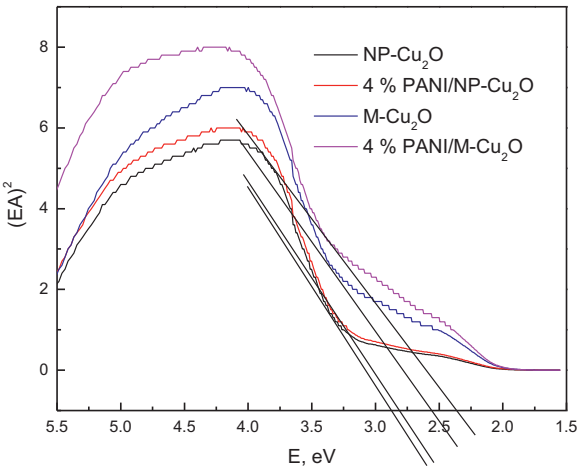


**Fig. 8.** Band gaps of the NP-$Cu_2O$, 4% PANI/NP-$Cu_2O$, M-$Cu_2O$, and 4% PANI/M-$Cu_2O$ samples.

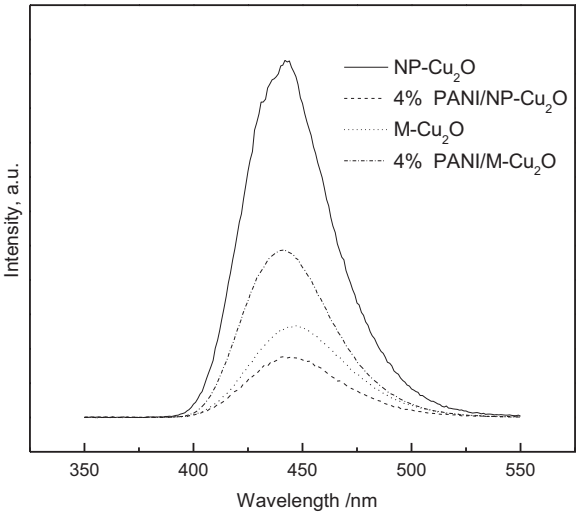


**Fig. 9.** PL spectra of the NP-$Cu_2O$, 4% PANI/NP-$Cu_2O$, M-$Cu_2O$, and 4% PANI/M-$Cu_2O$ samples.

wavelengths in the following order: NP-$Cu_2O$ to 4% PANI/NP-$Cu_2O$ to M-$Cu_2O$ to 4% PANI/M-$Cu_2O$. The band gaps were calculated as cited in previously published papers [32–34]. The band-gap values for the NP-$Cu_2O$, 4% PANI/NP-$Cu_2O$, M-$Cu_2O$, and 4% PANI/M-$Cu_2O$ are 2.87, 2.80, 2.56 and 2.37 eV, respectively, as shown in Fig. 8.

Fig. 9 shows the Pl spectra obtained for the NP-$Cu_2O$, 4% PANI/NP-$Cu_2O$, M-$Cu_2O$, and 4% PANI/M-$Cu_2O$ samples. The Pl intensity decreases in the following order: NP-$Cu_2O$ > 4% PANI/NP-$Cu_2O$ > M-$Cu_2O$ > 4% PANI/M-$Cu_2O$. PANI traps photogenerated electrons from the conduction band, separating the photogenerated e–h pairs. Loading PANI onto $Cu_2O$ enhanced the light absorption of the latter in the visible region, shifting the absorption edge toward longer wavelengths. Therefore, the band-gap energy decreased, incorporating additional photogenerated electrons and holes in the photocatalytic reactions.

### 3.7. The photocatalytic activity during thiophene degradation

#### 3.7.1. Effect of the type of photocatalyst

Fig. 10 shows the effect of the type of photocatalyst on the photocatalytic oxidation of thiophene. Photocatalytic tests were carried out using visible light under the following conditions: 0.4 g of photocatalyst and 500 mL of a 600 ppm thiophene solution. The

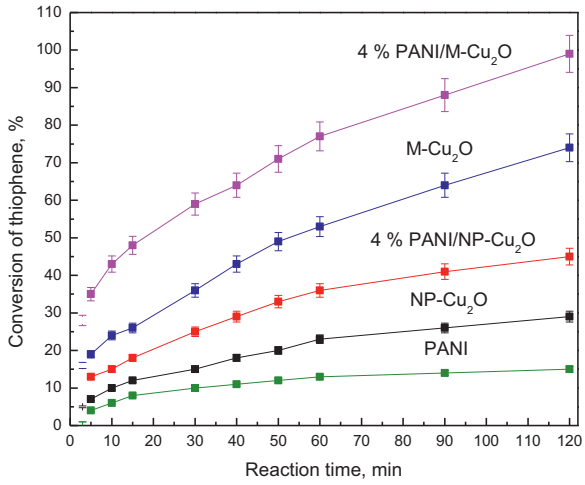


**Fig. 10.** The different catalyst types used for the photocatalytic degradation of thiophene.

**Table 1**
Quantum yields of PANI, NP-$Cu_2O$, 4% PANI/NP-$Cu_2O$, M-$Cu_2O$, and 4% PANI/M-$Cu_2O$.

| Photocatalysts | Quantum yield ($\Phi$) |
|---|---|
| PANI | 0.0100 |
| NP-$Cu_2O$ | 0.0200 |
| 4% PANI/NP-$Cu_2O$ | 0.0326 |
| M-$Cu_2O$ | 0.0800 |
| 4% PANI/M-$Cu_2O$ | 0.0990 |

photocatalytic activity % of the 4% PANI/M-$Cu_2O$ surpassed the activities of the M-$Cu_2O$, 4% PANI/NP-$Cu_2O$, and NP-$Cu_2O$ by 1.3, 2.2, and 3.4 times, respectively. Moreover, the quantum yield associated with the thiophene oxidation rate for 4% PANI/NP-$Cu_2O$ was approximately three times higher than that of 4% PANI/NP-$Cu_2O$, as shown in Table 1. Therefore, PANI/M-$Cu_2O$ displayed the highest photocatalytic activity. The band-gap values calculated for the NP-$Cu_2O$, 4% PANI/NP-$Cu_2O$, M-$Cu_2O$, and 4% PANI/M-$Cu_2O$ samples were 2.87, 2.80, 2.56, and 2.37 eV, respectively, as shown in Fig. 8.

To analyze the gases obtained from the photocatalytic process, the gases were passed over a sodium hydroxide solution (0.2 M). After adding a barium nitrate solution, a white precipitate formed (denoted as precipitate 1). Precipitate 1 was examined by XRD (Fig. S4A), confirming the formation of barium carbonate. Therefore, the thiophene was oxidized photocatalytically to form the carbon dioxide that was later trapped in the sodium hydroxide solution. After adding nitric acid to precipitate 1, a white precipitate did not dissolve in the nitric acid solution; this substance was labeled precipitate 2. Precipitate 2 was examined by XRD (Fig. S4B), confirming the formation of barium sulfate. Therefore, the sulfur in thiophene was photocatalytically oxidized to $SO_3$. The thiophene could be photocatalytically oxidized to form $CO_2$ and $SO_3$ as follows:

$$\text{Thiophene} + \text{photocatalyst} \rightarrow 2CO_2 + SO_3 + 2H_2O$$

Our results are in agreement with those reported in previous studies [35,36].

#### 3.7.2. Effect of the PANI content (wt%) on the photocatalytic activity of the PANI/M-$Cu_2O$ nanocomposite

Fig. 11 shows the effect of the PANI content (wt%) on the photocatalytic activity of PANI/M-$Cu_2O$ during the oxidation of thiophene. Increasing the PANI content from 1 to 4 wt% increased the photocatalytic activity from 81% to 100%, respectively. However, increasing the PANI content above 4 wt% decreased the photocatalytic activity because the PANI aggregated on the M-$Cu_2O$

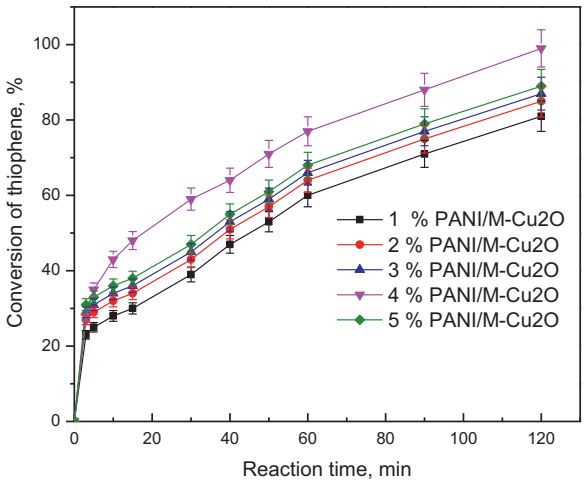


**Fig. 11.** Effect of the PANI content (wt%) on the photocatalytic degradation of thiophene.

surface, impeding e–h separation, in agreement with the results obtained for a PANI@$TiO_2$ system [21].

*3.7.3. Effect of the amount of the photocatalyst*

Another important factor affecting the photocatalytic activity process is the amount of photocatalyst. Photocatalytic tests were carried out using visible light under the following conditions: the amount of the 4% PANI/M-$Cu_2O$ photocatalyst was varied from 0.4 to 2.0 g, and 1000 mL of a 600 ppm thiophene solution was used. Fig. S5 shows the effect of the 4% PANI/M-$Cu_2O$ photocatalyst loading on the photocatalytic oxidation of thiophene. When the amount of 4% PANI/M-$Cu_2O$ was increased from 0.4 to 0.8 g/L, the photocatalytic activity increased from 84% to 100% after 120 min. Increasing the amount from 0.8 to 1.2 g/L decreased the reaction time from 120 to 60 min because using additional photocatalyst increases the number of active sites available for the photo-oxidation of thiophene, in agreement with the results obtained for a ZnO system [37]. Additionally, we observed that increasing the amount of 4% PANI/M-$Cu_2O$ above 1.2 g/L decreased the photocatalytic activity because the large amount of photocatalyst impeded the penetration of light through the photocatalyst, thus decreasing the catalyst's activity, in agreement with the results obtained for a UV/$TiO_2$/$H_2O_2$ system [38].

*3.7.4. Mechanism of photocatalytic oxidation of thiophene*

When the 4% PANI/M-$Cu_2O$ nanocomposite was irradiated by visible light, $Cu_2O$ absorbed photons and produced e–h pairs. In addition, PANI absorbed photons and produced $\pi$–$\pi^*$ pairs. Additionally, electrons excited by the irradiation of PANI transferred to the conduction band of $Cu_2O$, and holes produced by the irradiation of $Cu_2O$ transferred to the $\pi$ band of PANI. Therefore, PANI enhanced the separation of e–h pairs, and the photocatalytic activity of $Cu_2O$ increased. Based on the results obtained from the analysis of gas products and the band gap of the 4% PANI/M-$Cu_2O$ nanocomposite, the following reaction mechanism is proposed:

$$Cu_2O/PANI + Visiblelight \rightarrow Cu_2O/PANI^+ + e^-$$

$$e^- + O_2 \rightarrow O_2^-$$

$$O_2^- + 2e^- + 2H^+ \rightarrow OH + OH^-$$

$$h^+ + H_2O \rightarrow H^+ + OH^\bullet$$

$$Thiophene + OH^\bullet \rightarrow 2CO_2 + SO_3 + 2H_2O$$

*3.7.5. Recycling the photocatalyst*

Catalyst recycling is important when evaluating the practical application of photocatalysts and developing heterogeneous photocatalysts for wastewater treatment. The recycled 4% PANI/M-$Cu_2O$ catalyst converted 100% of the thiophene during the first five cycles as shown in Fig. S2. The XRD patterns of 4% PANI/M-$Cu_2O$ obtained before and after being reused five times were recorded as shown in Fig. 1. It was also observed that the shape of the composite XRD patterns after the first five cycles was similar to that observed before the reaction. This finding indicates that the structure of 4% PANI/M-$Cu_2O$ does not change during the photocatalytic process. In addition, the XPS patterns of 4% PANI/M-$Cu_2O$ before and after being reused five times were recorded as shown in Fig. 3. It was also observed that the shape of the composite XPS patterns after the first five cycles was similar to that observed before the reaction. This result indicates that the structure of 4% PANI/M-$Cu_2O$ does not change during the photocatalytic process. Therefore, this photocatalyst can be separated and recycled while maintaining its stability, making it a promising material for environmental remediation.

## 4. Conclusions

A PANI/M-$Cu_2O$ photocatalyst with a uniform core–shell structure was successfully prepared and characterized using FT-IR, XPS, BET, XRD, TEM, and UV–vis and PL spectroscopy. PANI is critical for the e–h separation process. The PANI/M-$Cu_2O$ nanocomposite photocatalyst can be used for thiophene photocatalytic degradation under visible-light irradiation. The photocatalytic activity of the 4% PANI/M-$Cu_2O$ photocatalyst could be optimized to yield 100% degradation of thiophene within 60 min of visible-light irradiation when using 1.2 g of the photocatalyst in 1000 mL of a 600 mg/L thiophene solution. The effectiveness and activity of the catalyst over five cycles revealed that the 4% PANI/M-$Cu_2O$ photocatalyst could be recycled.

## Appendix A. Supplementary data

Supplementary data associated with this article can be found, in the online version, at http://dx.doi.org/10.1016/j.apcata.2014.04.039.

## References

[1] H. Pang, F. Gao, Q.Y. Lu, CrystEngComm 12 (2010) 406–412.
[2] L. Huang, F. Peng, H. Yu, H. Wang, Solid State Sci. 11 (2009) 129–138.
[3] O. Akhavan, R. Azimirad, S. Safad, E. Hasani, J. Mater. Chem. 21 (2011) 9634–9640.
[4] O. Akhavan, E. Ghaderi, Surf. Coat. Technol. 205 (2010) 219–223.
[5] B. White, M. Yin, A. Hall, D. Le, S. Stolbov, T. Rahman, N. Turro, S. O'Brien, Nano Lett. 6 (2006) 2095–2098.
[6] J.H. Zhong, G.R. Li, Z.L. Wang, Y.N. Ou, Y.X. Tong, Inorg. Chem. 50 (2011) 757–763.
[7] M. Heinlaan, A. Ivask, I. Blinova, H.C. Dubourguier, A. Kahru, Chemosphere 71 (2008) 1308–1316.
[8] I. Perelshtein, G. Applerot, N. Perkas, E. Wehrschuetz-Sigl, A. Hasmann, G. Guebitz, A. Gedanken, Surf. Coat. Technol. 204 (2009) 54–57.
[9] L. Esteban-Tejeda, F. Malpartida, A. Esteban-Cubillo, C. Pecharrom'an, J.S. Moya, Nanotechnology 20 (2009) 505701.
[10] F. Gao, H. Pang, S.P. Xu, Q.Y. Lu, Chem. Commun. (2009) 3571–3573.
[11] C.H. Kuo, M.H. Huang, Nano Today 5 (2010) 106–116.
[12] H. Shi, K. Yu, F. Sun, Z.Q. Zhu, CrystEngComm 14 (2012) 278–285.
[13] X.Y. Meng, G.H. Tian, Y.J. Chen, Y. Qu, H.G. Fu, RSC Adv. 2 (2012) 2875–2881.
[14] K.X. Yao, X.M. Yin, T.H. Wang, H.C. Zeng, J. Am. Chem. Soc. 132 (2010) 6131–6144.
[15] S. Sun, C. Kong, S. Yang, L. Wang, X. Song, B. Ding, Z. Yang, CrystEngComm 13 (2011) 2217–2221.
[16] J. Dong, H. Xu, F. Zhang, C. Chen, L. Liu, G.T. Wu, Appl. Catal. A 470 (2014) 294–302.
[17] W. Wang, X. Huang, S. Wu, Y. Zhou, L. Wang, H. Shi, Y. Liang, B. Zou, Appl. Catal. B 134/135 (2013) 293–301.
[18] Y. Cao, Y. Xu, H. Hao, G. Zhang, Mater. Lett. 114 (2014) 88–91.
[19] L. Li, W. Zhang, C. Feng, X. Luan, J. Jiang, M. Zhang, Mater. Lett. 107 (2013) 123–125.

[20] C. Dong, M. Zhong, T. Huang, M. Ma, D. Wortmann, M. Brajdic, I. Kelbassa, ACS Appl. Mater. Interfaces 3 (11) (2011) 4332–4338.
[21] H. Zhang, R.L. Zong, J.C. Zhao, Y.F. Zhu, Environ. Sci. Technol. 42 (2008) 3803–3807.
[22] A. Hagfeldt, M. Graetzel, Chem. Rev. 95 (1995) 49–68.
[23] R.M. Mohamed, D.L. McKinney, W.M. Sigmund, Mater. Sci. Eng. R 73 (2012) 1–13.
[24] J.K. Mwaura, X.Y. Zhao, H. Jiang, K.S. Schanze, J.R. Reynolds, Chem. Mater. 18 (2006) 6109–6111.
[25] P.V. Kamat, J. Phys. Chem. C 112 (2008) 18737–18753.
[26] Q.F. Zhang, T.P. Chou, B. Russo, S.A. Jenekhe, G.Z. Cao, Angew. Chem. Int. Ed. 47 (2008) 2402–2406.
[27] Q.F. Zhang, T.P. Chou, B. Russo, S.A. Jenekhe, G.Z. Cao, Adv. Funct. Mater. 18 (2008) 1654–1660.
[28] H.J. Koo, Y.J. Kim, Y.H. Lee, W.I. Lee, K. Kim, N.G. Park, Adv. Mater. 20 (2008) 195–199.
[29] D.H. Chen, F.Z. Huang, Y.B. Cheng, R.A. Caruso, Adv. Mater. 21 (2009) 2206–2210.
[30] X. Wang, G. Chen, J. Zhang, Catal. Commun. 31 (2013) 57–61.
[31] F.Z. Huang, D.H. Chen, X.L. Zhang, R.A. Caruso, Y.B. Cheng, Adv. Funct. Mater. 20 (2010) 1301–1305.
[32] V. Kumar, S. Kr Sharma, T.P. Sharma, V. Singh, Opt. Mater. 12 (1999) 115–119.
[33] L. Korosi, I. Dekany, Colloids Surf. A 280 (2006) 146–154.
[34] S. Yao, X. Jia, L. Jiao, C. Zhu, Z. Shi, Indian J. Chem. 51 (2012) 1049–1056.
[35] X. Gao, F. Fu, L. Zhang, W. Li, Physica B: Condens. Matter 419 (2013) 80–85.
[36] F. Lin, Y. Zhang, L. Wang, Y. Zhang, D. Wang, M. Yang, J. Yang, B. Zhang, Z. Jiang, C. Li, Appl. Catal. B 127 (2012) 363–370.
[37] J. Nishio, M. Tokumura, H.T. Znad, Y. Kawase, J. Hazard. Mater. B138 (2006) 106–115.
[38] M. Saquib, M.A. Tariq, M.M. Haque, M. Muneer, J. Environ. Manage. 88 (2008) 300–306.